Ferromagnetic Kondo behavior in $UAuBi_2$ single crystals

P. F. S. Rosa,[1,2] Yongkang Luo,[3] E. D. Bauer,[3] J. D. Thompson,[3] P. G. Pagliuso,[1] and Z. Fisk[2]
[1]*University of California, Irvine, Irvine, California 92697-4574, U.S.A*
[2]*Instituto de Física "Gleb Wataghin," Campinas, SP 13083-859, Brazil*
[3]*Los Alamos National Laboratory, Los Alamos, New Mexico 87545, U.S.A.*
(Received 25 June 2015; published 22 September 2015)

We combine magnetization, pressure-dependent electrical resistivity, and heat capacity measurements to investigate the physical properties of the novel compound $UAuBi_2$. Our single crystals, grown by the self-flux method, share the same tetragonal $HfCuSi_2$-type structure as their Ce-based counterparts. $UAuBi_2$ shows ferromagnetic ordering at $T_c = 22.5$ K, in contrast with the antiferromagnetic transition found in $CeAuBi_2$ ($T_N = 12$ K) but closely related to $UAuSb_2$ ($T_c = 31$ K). Despite the differences, all compounds display an easy axis of magnetization along the c axis and a large magnetocrystalline anisotropy. The heat capacity and pressure-dependent resistivity suggest that $UAuBi_2$ exhibits moderately heavy-fermion behavior ($\gamma \sim 100$ mJ/mol $\cdot$ K^2) with strongly localized $5f$ electrons. An intricate competition between crystalline electric field (CEF) effects and two anisotropic exchange interactions (J_{RKKY}) persists in the $5f$ system, which leads to the striking difference between ground states. A systematic analysis of our macroscopic data using a mean-field model including anisotropic J_{RKKY} interactions and the tetragonal CEF Hamiltonian allows us to extract the CEF scheme and the values of J_{RKKY}. Our results suggest a general trend in this family of compounds and shed light on the similarities and differences between $4f$ and $5f$ members.

DOI: 10.1103/PhysRevB.92.104425 PACS number(s): 75.20.Hr, 74.62.Fj, 75.10.Dg, 75.50.Cc

I. INTRODUCTION

The magnetism of actinide-based compounds is often complex due to an intricate competition among the Ruderman-Kittel-Kasuya-Yosida (RKKY) magnetic interaction, crystalline electrical field (CEF) effects, the Coulomb interaction, and hybridization between the rather extended $5f$ electrons and the conduction electrons. Interesting physical phenomena may arise from this interplay, such as heavy-fermion (HF) behavior and unconventional superconductivity in UBe_{13}, quadrupolar ordering in UPd_3, and antiferromagnetism in $UNiGa_5$ [1–3]. Unveiling the effect of each interaction on the ground state is a nontrivial task which constantly motivates further research. In this regard, the study of novel compounds represents a great opportunity to shed new light on the current understanding of the properties of a given series of compounds.

In this context, here we revisit the UMX_2 family (M = transition metal, X = pnictogen) by probing and simulating the macroscopic properties of a novel member with M = Au and X = Bi. Great attention has been paid previously to the magnetism of X = P, As, and Sb members of this family [4–12]. For instance, antimonides with M = Co, Cu, Ag, and Au have been found to order ferromagnetically, while those with M = Ni, Ru, andPd have antiferromagnetic (AFM) order at low T [12]. The observed variety of magnetic ordering in these series has been attributed to both superexchange and RKKY exchange interactions due to f-p and f-d hybridization, respectively. In particular, the strong anisotropy, a common feature in this family, has been ascribed to a pronounced f-p mixing, whereas the type of magnetic ordering is presumably correlated with the magnitude of f-d overlap. Concerning the X = Bi members, although Ce-based bismuthides have recently attracted considerable attention, studies on the $UTBi_2$ series are rather scarce. To the best of our knowledge, only polycrystalline samples with M = Cu and Ni have been reported [13]. Magnetization data show evidence of AFM order below $T_N = 51$ and 166 K, respectively. In particular, a detailed quantitative analysis of the relevant interactions in U-based members is still missing.

Quantitative analyses have been performed in recent reports on $CeMBi_2$ (M = Cu, Au), which present AFM ordering at $T_N = 16$ K (Cu) and $T_N = 12$ K (Au) [14,15]. Using a mean-field model with contributions of anisotropic first-neighbor interactions and the tetragonal CEF [16], the experimental properties were well reproduced by an appropriate CEF scheme. Furthermore, these Ce-based systems have been shown to exhibit a moderately HF behavior with strongly localized Ce^{3+} $4f$ electrons. A straightforward question that arises is how the uranium members would behave with their rather extended $5f$ bands. Hence, the investigation of the $UAuBi_2$ compound is a suitable choice to explore the effects of delocalization of the f bands in this structurally related series of compounds.

Here we report the synthesis and physical properties of $UAuBi_2$ single crystals by means of magnetization, heat capacity, and pressure-dependent electrical resistivity. $UAuBi_2$ is an intermetallic compound which crystallizes in a tetragonal $HfCuSi_2$-type structure ($P4/nmm$) with a stacking arrangement of UBi-Au-UBi-Bi layers. Our results reveal a strongly uniaxial ferromagnetic (FM) ordering at $T_c = 22.5$ K, with the easy axis of magnetization along the c axis. As carried out on Ce-based members, we extracted the CEF scheme and the anisotropic RKKY interactions which best describe the properties of $UAuBi_2$. Furthermore, the combined analyses of specific heat- and pressure-dependent electrical resistivity suggest a scenario where $UAuBi_2$ displays incoherent Kondo behavior with rather localized U^{3+} $5f$ electrons.

II. EXPERIMENTAL DETAILS

Single crystals of $UAuBi_2$ and $ThAuBi_2$ (a nonmagnetic reference) were grown from Bi flux with a starting composition

of U/Th:Au:Bi = 1:3:20. The crucible containing the elements was sealed inside an evacuated quartz tube, which was then heated up to 1050 °C for 8 h, cooled to 800 °C over 3 h, and, finally, slowly cooled down at 5 °C/h. The excess of Bi flux was removed at 450 °C by centrifugation and platelet-like crystals were mechanically removed from the crucible [17]. The excess of Au is used to avoid the formation of the superconducting binary $AuBi_2$ as well as to avoid a deficiency at the transition metal site, as observed previously in $CeAu_{0.92}Bi_{1.6}$ single crystals grown at the initial stoichiometry 1:1:20 [15]. It is noteworthy that vacancies have also been reported in several antimonide single crystals [9–11].

The crystallographic structure was verified by x-ray powder diffraction and the extracted lattice parameters are $a = 4.610(1)$ Å and $c = 9.610(2)$ Å. In addition, several samples were submitted to elemental analysis using a commercial energy dispersive spectroscopy microprobe. The obtained stoichiometry is 1:1:1.9, with an error of 5%. Although only cleaved samples were used in our measurements, we attribute the Bi deficiency to the high air sensitivity of the crystals, which likely induces the formation of thin layers of Bi oxide on the surface.

Magnetization measurements were performed using a commercial superconducting quantum interference device (SQUID). The specific heat was measured using a commercial small-mass calorimeter that employs a quasiadiabatic thermal relaxation technique. Electrical resistance was measured by the standard four-probe technique. A piston-clamp -type pressure cell was used to pressurize the sample, and Daphne oil 7373 was employed as a pressure-transmitting medium. Hydrostatic pressure up to 2.13 GPa was applied in the experiment, during which highly pure Pb was used as the manometer.

III. RESULTS AND DISCUSSION

Figure 1(a) shows the temperature dependence of the magnetic susceptibility, $\chi(T)$, in the paramagnetic state ($T > T_c$) when $H = 1$ kOe is applied parallel, $\chi_\parallel$ (open circles), and perpendicular, $\chi_\perp$ (open triangles), to the crystallographic c axis. The non-f contribution was subtracted from the data using the nonmagnetic reference compound $ThAuBi_2$. Above 150 K, $\chi(T)$ can be well fit by a Curie-Weiss (CW) term, $\chi(T) = C/(T - \theta_{CW})$, which gives the linear behavior shown by $1/\chi(T)$ [right inset in Fig. 1(a)]. The effective moment and θ values are considerably anisotropic: $\mu_{||} = 3.3(1)\mu_B$, $\mu_\perp = 3.6(1)\mu_B$, $\theta_{||} = 8$ K, and $\theta_\perp = -115$ K. In the simplest approximation using a molecular field in the absence of CEF effects, the anisotropy of θ indicates the presence of two effective exchange interactions with opposite signs (i.e., FM and AFM) between U moments. Although we show below that CEF effects are important, we note that anisotropic interactions have been observed previously in UMX_2 (X = As, Sb) compounds by neutron diffraction [5,12]. More recently, it has been shown by x-ray resonant magnetic scattering in the AFM $CeCuBi_2$ compound that the magnetic moments are aligned parallel tothe c-axis with $(++--)$ coupling [14]. Thus, anisotropic exchange parameters appear to be an intrinsic characteristic in this series of compounds.

The polycrystalline averaged susceptibility, $\chi_{poly}(T)$ (not shown), gives in turn $\theta_p = 12$ K, consistent with FM ordering.

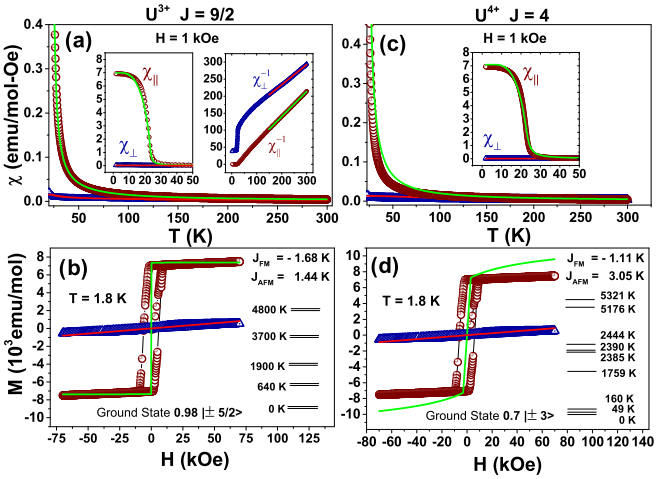

FIG. 1. (Color online) (a) Temperature dependence of the magnetic susceptibility measured with $H = 1$ kOe applied parallel, $\chi_\parallel$, and perpendicular, $\chi_\perp$, to the c axis. Left inset: FM transition at 22.5 K. Right inset: Inverse susceptibility. (b) Magnetization as a function of the magnetic field applied parallel (open circles) and perpendicular (open triangles) to the c axis at $T = 1.8$ K. Solid lines are the best fits of the data to the U^{3+} CEF mean-field model. (c, d) The same data as displayed in (a) and (b), with the best fits assuming a U^{4+} scheme.

In the left inset in Fig. 1(a), one can clearly observe the magnetic transition at $T_c = 22.5$ K, particularly in the $\chi_\parallel$ data, which is consistent with an easy axis along the c direction. The drastic anisotropy in the susceptibility data gives rise to a ratio of $\chi_\parallel/\chi_\perp \approx 135$ at T_c, which in turn suggests the presence of a large tetragonal CEF splitting and a large single-ion magnetic anisotropy.

Figure 1(b) displays the field-dependent magnetization, $M(H)$, at 1.8 K. The squared hysteresis curve observed when the $H \parallel c$ axis, typical of hard magnets, displays a coercive field of ∼6 kOe. A less squared hysteresis with a coercive field of ∼11 kOe is observed for the $H \perp c$ axis and saturation is not reached for fields up to $H = 70$ kOe. The solid lines in Figs. 1(a) and 1(b) represent the best fits using a CEF mean-field model assuming the U^{3+} ($J = 9/2$, $S = 3/2$) configuration discussed in detail below. Figures 1(c) and 1(d) display the same data as in Figs. 1(a) and 1(b) with the corresponding fits of a U^{4+} ($J = 4$, $S = 1$) configuration.

To establish a plausible scenario for the magnetic properties of $UAuBi_2$, we have analyzed the data presented in Figs. 1 and 2 using a mean-field model including two anisotropic interactions between nearest neighbors as well as the tetragonal CEF Hamiltonian, given by

$$H_{CEF} = B_2^0 O_2^0 + B_4^0 O_4^0 + B_4^4 O_4^4 + B_6^0 O_6^0 + B_6^4 O_6^4, \quad (1)$$

where B_i^n are the CEF parameters and O_i^n are the Stevens equivalent operators obtained from the angular momentum operators [16,18]. For instance, the operator $O_{2,i}^0 = 3\hat{J}_{z,i}^2 - J(J+1)$ favors in-plane alignment of spins (i.e., $\hat{J}_z = 0$) if $B_2^0 > 0$. Analogously, if $B_2^0 < 0$, there is a tendency toward alignment along the c axis. For a complete description of the theoretical model, see Ref. [16]. It is possible to fit our data with either U^{4+} or U^{3+} schemes. However, as one can see in Fig. 1, the fit that best reproduces the anisotropy at high

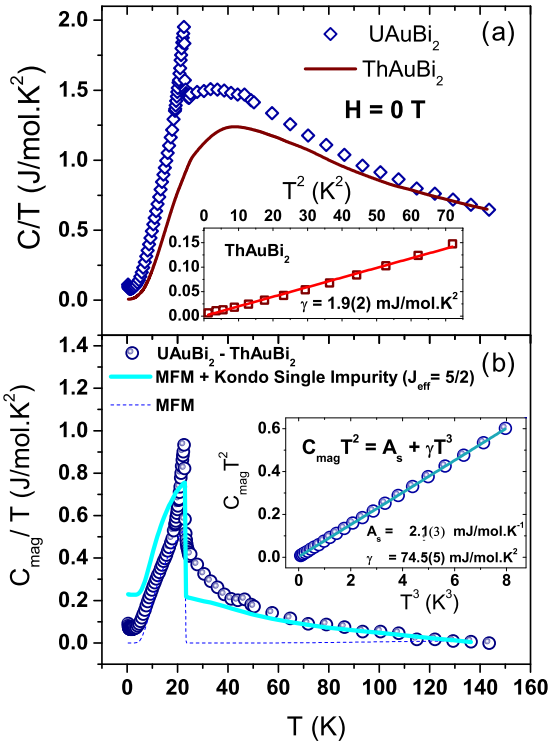

FIG. 2. (Color online) (a) Temperature dependence of the specific heat of $UAuBi_2$ and its nonmagnetic reference compound $ThAuBi_2$. Inset: A linear fit of $C(T)/T$ vs T^2 for $ThAuBi_2$. (b) Magnetic contribution to the specific heat of $UAuBi_2$ as a function of the temperature and the corresponding fits using a mean-field model (dashed lines) and an additional single-impurity term (solid lines). Inset: A linear fit to the data in a CT^2-vs-T^3 plot.

and low temperatures, the FM transition temperature, and the magnetization saturation in the ground state is obtained for the 3+ case.

The extracted CEF parameters, exchange interactions, and corresponding eigenvalues and eigenfunctions for the 3+ scheme are listed in Table I. As expected, two RKKY parameters with opposite signs but similar amplitudes are found, suggesting a strong competition between FM and AFM ground states. Furthermore, it becomes clear that the large anisotropy in χ is caused by the large value of B_2^0, which in turn gives rise to the substantial overall splitting of ~5000 K. It is worth noting that, independent of the uranium scheme, the large splitting, the anisotropic interactions, and the large value of B_2^0 are always observed. We also note that CEF splittings of the same order have been observed in several low-symmetry compounds in the large-moment regime, such as UNi_2Al_3, URu_2Si_2, $UCuAs_2$, and UAsSe [6,19–21].

In order to gather more insightinto the HF nature of $UAuBi_2$, we now turn our attention to the temperature dependence of its specific heat at zero field. Figure 2(a) displays the specific heat of $UAuBi_2$ and its nonmagnetic reference compound $ThAuBi_2$.The inset in Fig. 2(a) shows the small Sommerfeld coefficient, $\gamma = 1.9(2)$ mJ/mol · K^2, obtained for the Th member. The magnetic specific heat $C_{\rm mag}(T)/T$ of $UAuBi_2$ is then obtained after subtracting the lattice contribution from $ThAuBi_2$, as shown in Fig. 2(b). The peak of $C_{\rm mag}(T)/T$ defines $T_c = 22.5$ K consistently with the FM transition temperature observed in magnetization measurements. From the $C_{\rm mag}(T)/T$ data it is possible to estimate the Sommerfeld coefficient γ of $UAuBi_2$ by performing an entropy-balance construction $[S(T_c - \epsilon) = S(T_c + \epsilon)]$. Thus, we obtain $\gamma \sim$ 100–150 mJ/mol · K^2, indicating that $UAuBi_2$ is a moderately HF compound.

As the temperature is lowered further, an upturn of $C_{\rm mag}(T)/T$ is observed below ~1 K, which can be well fit by a sum of both electronic (γ) and nuclear Schottky ($\propto T^{-3}$) terms [22]. These contributions give rise to a straight line in a CT^2-vs-T^3 plot, as shown in the inset in Fig. 2, which allows us to extract the electronic coefficient $\gamma = 75$ mJ/mol · K^2, in agreement with our previous entropy-balance estimate. We note that a nuclear Schottky term is expected due to the large nuclear quadrupole moments of bismuth [23].

Interestingly, in contrast with the analyses performed for Ce members, we are not able to fit satisfactorily the high-

TABLE I. CEF parameters, energy levels, and wave functions obtained from the best fits of magnetic susceptibility data on $UAuBi_2$ single crystals. Here, $z_{\rm AFM}$ ($z_{\rm FM}$) are the U^{3+} nearest neighbors with an AFM (FM) coupling, in this case, 2 (4).

CEF parameter (K)										
		B_2^0	B_4^0	B_4^4	B_6^0	B_6^4	$z_{\rm FM}J_{\rm FM}$	$z_{\rm AFM}J_{\rm AFM}$		
		22.65	1.20	0.72	−0.007	0.02	−1.68	1.44		
Energy levels and wave functions										
E (K)	$\lvert -9/2\rangle$	$\lvert -7/2\rangle$	$\lvert -5/2\rangle$	$\lvert -3/2\rangle$	$\lvert -1/2\rangle$	$\lvert +1/2\rangle$	$\lvert +3/2\rangle$	$\lvert +5/2\rangle$	$\lvert +7/2\rangle$	$\lvert +9/2\rangle$
0	0.00	−0.13	0.00	−0.10	0.00	0.00	0.00	0.986	0.00	0.00
0	0.00	0.00	0.986	0.00	0.00	0.00	−0.10	0.00	−0.13	0.00
640	0.00	0.00	0.13	0.00	0.00	0.00	0.00	0.00	0.989	0.00
640	0.00	−0.989	0.00	0.00	0.00	0.00	0.00	−0.13	0.00	0.00
1930	0.00	0.00	0.10	0.00	0.00	0.00	0.994	0.00	0.00	0.00
1930	0.00	0.00	0.00	−0.994	0.00	0.00	0.00	−0.10	0.00	0.00
3750	0.00	0.00	0.00	0.00	0.00	0.994	0.00	0.00	0.00	−0.10
3750	−0.1	0.00	0.00	0.00	−0.994	0.00	0.00	−0.10	0.00	0.00
4750	0.00	0.00	0.00	0.00	0.00	0.1	0.00	0.00	0.00	0.995
4750	0.995	0.00	0.00	0.00	0.10	0.00	0.00	0.00	0.00	0.00

temperature behavior of $C_{\rm mag}(T)/T$ (dashed lines in Fig. 2) using the same parameters obtained from the magnetic susceptibility data. Entropy deficits usually point to an additional interaction that was not addressed by the original model. We note that our initial Hamiltonian accounts for the main features of the data shown in Fig. 1 because the anisotropy of χ is mainly given by the CEF parameter B_2^0 and the FM-order ground state is a result of the interplay between the CEF scheme and the anisotropic exchange interactions. Although Kondo fluctuations do not play a fundamental role in the analysis of χ, they may be important when simulating specific heat data. In fact, we see below that $UAuBi_2$ presents a classic Kondo-type behavior in resistivity ($\rho \propto -\ln T$) above T_c, indicating that a Kondo effect is indeed present. It is noteworthy that an entropy deficit is also observed in the U^{4+} scheme.

As a first approximation, we now include a Kondo single-impurity term for an impurity with total angular momentum J, as calculated by Rajan [24]. Although a perfect agreement between calculated and experimental values is unlikely here because $UAuBi_2$ is a dense Kondo lattice and short-range interactions may be present, we find a much better agreement with the experimental data (solid lines in Fig. 2). Interestingly, the calculated specific heat with $J_{\rm eff} = 5/2$ gives the best results, which suggests that the main Kondo contribution comes from the three low-energy doublets. The Kondo temperature extracted from the fits, $T_K^0 = 100$ K, is an effective temperature for $J_{\rm eff} = 5/2$; i.e., individual CEF doublets may have different values of T_K. We note that the effective value found here for $UAuBi_2$ is comparable to the values found for UNi_2Al_3 ($T_K \sim 72$ K) by optical reflectance spectroscopy and for URu_2Si_2 ($T_K \sim 129$ K) by scanning tunneling microscopy [25,26].

Although the obtained CEF parameters combined with the anisotropic exchange constants and the Kondo single-impurity term account for the main features of the data shown in Figs. 1 and 2, the parameters extracted from fits to macroscopic measurement data may not be unique and/or extremely precise. It will be valuable to compare our CEF scheme with accurate experimental determinations of the CEF scheme by inelastic neutron scattering, for example [27]. Nonetheless, apart from a more precise determination of the CEF parameters, the analysis presented here suggests that the U $5f$ electrons behave as localized U^{3+} magnetic moments subjected to dominant CEF effects and anisotropic RKKY interactions.

As applied pressure is well known to favor the Kondo effect with respect to the RKKY interaction in HF compounds, we now turn our attention to pressure-dependent electrical resistivity measurements to further investigate the Kondo lattice behavior in $UAuBi_2$. First, the field-dependent in-plane electrical resistivity data at ambient pressure, $\rho(T, P = 0)$, are summarized in Fig. 3. At zero field, $\rho(T, P = 0)$ displays a typical Kondo behavior in the paramagnetic regime (open squares). Above 40 K, $\rho(T, P = 0)$ can be well described by the function

$$\rho(T) = \rho_0^{\rm HT} - c_K \ln T, \qquad (2)$$

where $\rho_0^{\rm HT}$ is the disorder scattering term and c_K is the logarithmic Kondo term. From a least squared fit of the data to this equation [solid lines in Fig. 3(b)], we obtain $\rho_0^s = 1.3(3)$ m$\Omega \cdot$ cm and $c_K = 0.153(1)$ m$\Omega \cdot$ cm, thus hinting at a substantial disorder and an enhanced $J_{fs}N(E_F)$, respectively. Here J_{fs} is the exchange interaction between $5f$ and conduction electrons and $N(E_F)$ is the density of states at the Fermi level, E_F. We note that these values agree with previous reports on U-based 112 systems, such as $UPdSb_2$, $UCuAs_2$, and $UCuSb_2$ [11,12,28]. More generally, the relatively large absolute values of resistivity appear to be a common trend in RTX_2 (R = Ce, U) compounds. For instance, $CeAuBi_2$ displays $\rho = 0.16$ m$\Omega \cdot$ cm at 300 K, although no logarithmic Kondo behavior is observed at high temperatures [15]. This is likely related to a relatively small number of carriers, i.e., small Fermi surfaces. Band structure calculations would be a valuable tool to test this hypothesis.

As the temperature is further lowered, $\rho(T)$ displays a sharp drop at 23.5 K due to the onset of FM order. Interestingly, T_c has also a clear signature in the magnetoresistance (MR), defined as $\Delta\rho/\rho_0(\%) = [\rho(H = 90\ {\rm kOe}, T) - \rho(H = 0\ {\rm kOe}, T)] \times 100/\rho(0, T)$, with H applied along the c axis. As one can observe in the inset in Fig. 3(a), $\Delta\rho/\rho_0$ shows a sharp negative minimum, likely due to the suppression of the spin fluctuations as a function of the applied field near the transition temperature. Below $T \sim 9$ K, however, the MR becomes positive, which may be attributed to two phenomena. First, positive MR often points to the presence of AFM interactions. In fact, two sign-changing exchange interactions

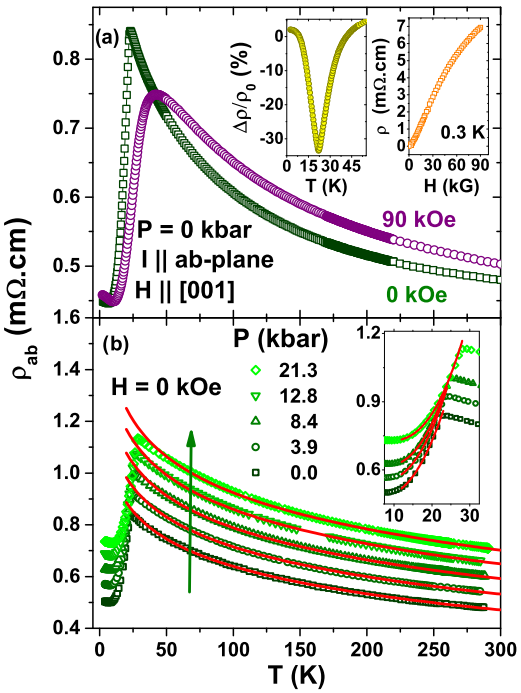

FIG. 3. (Color online) (a) Temperature dependence of the electrical resistivity, $\rho(T)$, at $H = 0$ and 90 kOe. Right inset: Resistivity at 0.3 K as a function of the magnetic field. Left inset: Temperature dependence of magnetoresistance, defined as $\Delta\rho/\rho_0(\%) = [\rho(H = 90\ {\rm kOe}, T) - \rho(H = 0\ {\rm kOe}, T)] \times 100/\rho(0, T)$. (b) $\rho(T)$ for different values of applied hydrostatic pressure up to 21 kb. An offset of 0.05 m$\Omega \cdot$ cm was used for clarity. Solid lines display the best fits of the data to Eq. (2). Inset: Low-T behavior for selected pressures and the corresponding fits (solid lines) to Eq. (3).

TABLE II. Extracted parameters from fits of pressure-dependent resistivity data to Eqs. (2) and (3) at high and low temperatures, respectively.

Pressure (kb)	T_c^{onset} (K)	T_{min} (K)	ρ_0^{HT} (m$\Omega \cdot$ cm)	c_K (m$\Omega \cdot$ cm)	ρ_0 (m$\Omega \cdot$ cm)	D (m$\Omega \cdot$ cm)	Δ (K)
0	23.5	7.5	1.3(3)	0.153(1)	0.478(6)	0.9(2)	31(2)
3.9	24.4	7.7	1.4(3)	0.166(1)	0.497(3)	1.2(2)	36(1)
8.4	25.7	8.1	1.5(3)	0.179(1)	0.513(1)	1.9(1)	43.7(9)
12.7	27.2	8.7	1.6(3)	0.192(1)	0.524(1)	2.7(1)	49.9(6)
18.6	28.3	9.1	1.7(4)	0.201(1)	0.528(1)	3.1(1)	54.1(6)
21.3	28.7	9.2	1.7(4)	0.203(1)	0.524(1)	3.1(1)	55.2(5)

with comparable absolute values need to be included in our mean-field model to fit the macroscopic data well. Second, the tendency of saturation of the MR isotherm [right inset in Fig. 3(a)] indicates that positive MR may be due to the presence of closed orbits in an uncompensated metal.

The evolution of $\rho(T)$ as a function of the pressure is shown in Fig. 3(b) and the parameters obtained from fitting the data to Eq. (2) are listed in Table II. We observe that both the ρ_0^{HT} and the c_K terms increase with pressure, signaling to an increase in the product $J_{fs}N(E_F)$. Consequently, the Curie temperature also increases from $T_c^{\text{onset}} = 23.5$ K at ambient pressure up to 28.7 K at 21 kb, suggesting that the U^{3+} $5f$ electrons remain rather localized in the studied pressure range. It is noteworthy that $UAuSb_2$ orders at $T_c = 36$ K, suggesting that applied and chemical pressure have the same effect.

Below T_c, ρ(T) cannot be fitted by a Fermi-liquid (FL) T^2 term, suggesting that FM magnons may be present. In fact, the electrical resistivity in the FM state can be reproduced over a wider temperature range by the expression

$$\rho(T) = \rho_0 + AT^2 + D\frac{T}{\Delta}\left(1 + \frac{2T}{\Delta}\right)e^{-\Delta/T}. \qquad (3)$$

In this equation, the first two terms describe the usual FL expression where ρ_0 is the residual resistivity and A is the FL coefficient proportional to the mass of the quasiparticles. The third term is the contribution due to an energy gap in the magnon dispersion relation, where D is related to the electron-magnon and spin disorder scattering and Δ is the magnitude of the gap [29]. The inset in Fig. 3 shows the best fits of the data to Eq. (3) using a fixed temperature window between 12 and 23 K. A deviation from Eq. (3) is observed below $T \sim 12$ K and a small upturn in $\rho(T)$ starts to develop below ~9 K. Due to the presence of this upturn, it was necessary to exclude the lowest temperature data from the magnon fits. The evolution of the fitted parameters as a function of pressure is reported in Table II. Interestingly, the FL coefficient A vanishes for all values of applied pressure, suggesting that the dominant contribution to the scattering comes from the electron-magnon term. The energy gap Δ in the magnon dispersion relation increases from 32 to 55 K, in agreement with the increase in T_c.

Now we are able to compare the obtained CEF scheme for $UAuBi_2$ with the one for the Ce-based parent compounds $CeAu_{1-\delta}Bi_2$ (AFM) and $CeCd_{1-\delta}Bi_2$ (FM), as reported in Table III. We first note that the ratio between the susceptibility along the easy axis and the susceptibility along the hard axis, $\chi_{\text{easy}}/\chi_{\text{hard}}$, is mainly determined by the tetragonal CEF parameter B_2^0 and it reflects the low-T single-ion anisotropy of Ce and U ions. In fact, we observe in Table III that higher $\chi_{\text{easy}}/\chi_{\text{hard}}$ values are accompanied by an increase in $|B_2^0|$. We return to the sign of B_2^0 below. At this point, it becomes clear that there is also an enhancement of the magnetic transition temperature (either T_c or T_N) with $|B_2^0|$ and the low-temperature magnetic anisotropy. In particular, we find that the crystal-field ground-state doublet becomes more isolated from the excited states as $T_{c,N}$ increases. Interestingly, it has recently been shown that a systematic enhancement of the AFM transition temperature (T_N) is also realized in the series $CeNi_{1-x}Bi_2$ as a function of x, due to the increase in the B_2^0 parameter and the low-T Ce^{3+} magnetic anisotropy [30]. Hence, a general trend emerges in the 112 family due to subtle changes in the CEF scheme. In particular, the large magnetic anisotropy of the U member, in comparison with the Ce members, can be explained by the large separation between the ground state and the first excited state ($\Delta_{\text{CEF}}^1 = 640$ K), which is ~5 times larger than the values typically found in Ce members [14,15,31,32].

Finally, we would like to comment on the sign of B_2^0. It is well known that, by using the high-temperature expansion of the magnetic susceptibility, the value of B_2^0 can be written in terms of the paramagnetic Curie-Weiss temperatures as $B_2^0 = (10/3)(\theta_{ab} - \theta_c)/(2J-1)(2J+3)$. This estimate gives a negative value of B_2^0, which is in apparent contradiction with the results presented here for $UAuBi_2$. However, we note that the above equation is only valid for isotropic interactions, which is clearly not the case for the 112 family of compounds. It is also noteworthy that, when $B_2^0 > 0$, the operator $O_{2,i}^0 = 3\hat{J}_{z,i}^2 - J(J+1)$ favors in-plane alignment of spins, and when $B_2^0 < 0$, c-axis alignment is favorable. Thus, an Ising-type AFM would be expected in the $CeTBi_2$ family,

TABLE III. Comparison among the extracted parameters for $CeAu_{0.92}Bi_{1.6}$[15], $CeCd_{1-\delta}Sb_2$ [31], and $UAuBi_2$ (this work).

	$T_{c/N}$ (K)	$\chi_{\text{easy}}/\chi_{\text{hard}}$	B_2^0 (K)	B_4^0 (K)	B_4^4 (K)	$z_{\text{AFM}}J_{\text{AFM}}$ (K)	$z_{\text{FM}}J_{\text{FM}}$ (K)
$CeAu_{1-\delta}Bi_2$	12 (AFM)	17 (c)	−15.57	0.01	0.76	1.4	−1.1
$CeCd_{1-\delta}Sb_2$	3 (FM)	15 (ab)	10.9	−0.4	−2.83	0.1	−12.1
$UAuBi_2$	22.5 (FM)	135 (c)	22.65	1.20	0.72	1.4	−1.7

which is exactly what is observed experimentally [14,15]. On the other hand, in-plane alignment of spins would be expected in the antimonide compounds $CeCd_{1-\delta}Sb_2$ and $CeAgSb_2$, for example, as well as in the U-based compound studied here. Although this is the case for $CeCd_{1-\delta}Sb_2$, both $CeAgSb_2$ and $UAuBi_2$ have their ordered moment along the c axis. It has been argued previously for $CeAgSb_2$ that, when the exchange interaction has a strong Ising character ($J_z \gg J_{x,y}$), the magnetic ordering of the z component, $\hat{J}_z$, can take over the ordering of the in-plane components $\hat{J}_x$ and $\hat{J}_y$. We believe that this is also the case for $UAuBi_2$.

IV. CONCLUSIONS

In summary, the magnetic, electrical, and thermal properties of $UAuBi_2$ are investigated by means of temperature-dependent magnetic susceptibility, pressure-dependent electrical resistivity, and heat capacity measurements. Our data reveal that $UAuBi_2$ orders ferromagnetically at $T_c = 22.5$ K, with the easy axis of magnetization along the c axis. A detailed analysis of the macroscopic properties was performed using a mean-field model with two anisotropic exchange interactions and the tetragonal CEF. Our approach allowed us to obtain the CEF scheme that best fits the macroscopic data. We note, however, that for a precise determination of the CEF parameters and wave functions a more direct spectroscopic technique is needed. Nevertheless, our results shed light on the evolution of the magnetic anisotropy presented in the 112 family of compounds, including Ce and U members. In particular, we find that the magnetic ordering temperature (either T_c or T_N) increases with the CEF parameter $|B_2^0|$, implying a larger magnetic anisotropy and larger separation between the ground state and the first excited state. The combined analyses in this investigation suggest that, as in the Ce-based members, $UAuBi_2$ presents localized f electrons subjected to dominant CEF effects and anisotropic RKKY interactions. As such, one may speculate that the strong local moment character of the magnetism in the 112 family is a dominant trend, which in turn does not favor the emergence of superconductivity in this family.

ACKNOWLEDGMENTS

We thank Prof. R. R. Urbano (Unicamp-Brazil) and H. Sakai (ASRC-Japan) for suggesting useful references. This work was supported by FAPESP (Grant Nos. 2013/17427-7 and 2012/04840-7) and CNPq (Grant Nos. 442230/2014-1 and 304649/2013-9). Work at Los Alamos was performed under the auspices of the U.S. Department of Energy, Office of Basic Energy Sciences, Division of Materials Science and Engineering. Y. Luo acknowledges a Director's Postdoctoral Fellowship supported through the Los Alamos LDRD program.

[1] H. R. Ott, H. Rudigier, Z. Fisk, and J. L. Smith, Phys. Rev. Lett. **50**, 1595 (1983).
[2] Y. Tokiwa, K. Sugiyama, T. Takeuchi, M. Nakashima, R. Settai, Y. Inada, Y. Haga, E. Yamamoto, K. Kindo, H. Harima *et al.*, J. Phys. Soc. Jpn. **70**, 1731 (2001).
[3] N. O. Moreno, E. D. Bauer, J. L. Sarrao, M. F. Hundley, J. D. Thompson, and Z. Fisk, Phys. Rev. B **72**, 035119 (2005).
[4] P. Fumagalli, J. Schoenes, and D. Kaczorowski, Solid State Commun. **65**, 173 (1988).
[5] P. Fischer, A. Murasik, D. Kaczorowski, and R. Troć, Physica B **156-157**, 829 (1989).
[6] D. Kaczorowski and R. Troc, J. Phys.: Condens. Matter **3**, 4959 (1991).
[7] H. Noël, Z. Zołnierek, D. Kaczorowski, and R. Troć, J. Less Common Metals **132**, 327 (1987).
[8] D. Kaczorowski, H. Noël, and M. Potel, J. Alloys Compds. **302**, 1 (2000).
[9] Z. Bukowski, D. Kaczorowski, J. Stepien Damm, D. Badurski, and R. Troć, Intermetallics **12**, 1381 (2004).
[10] Z. Bukowski, V. Tran, J. S. Damm, and R. Troć, J. Solid State Chem. **177**, 3934 (2004).
[11] Z. Bukowski, R. Troć, J. Stepien Damm, C. Sułkowski, and V. Tran, J. Alloys Compds. **403**, 65 (2005).
[12] D. Kaczorowski, R. Kruk, J. P. Sanchez, B. Malaman, and F. Wastin, Phys. Rev. B **58**, 9227 (1998).
[13] D. Kaczorowski, J. Alloys Compds. **186**, 333 (1992).
[14] C. Adriano, P. F. S. Rosa, C. B. R. Jesus, J. R. L. Mardegan, T. M. Garitezi, T. Grant, Z. Fisk, D. J. Garcia, A. P. Reyes, P. L. Kuhns *et al.*, Phys. Rev. B **90**, 235120 (2014).
[15] C. Adriano, P. F. S. Rosa, C. B. R. Jesus, T. Grant, Z. Fisk, D. J. Garcia, and P. G. Pagliuso, J. Appl. Phys. **117**, 17C103 (2015).
[16] P. G. Pagliuso, D. J. Garcia, E. Miranda, E. Granado, R. Lora Serrano, C. Giles, J. G. S. Duque, R. R. Urbano, C. Rettori, J. D. Thompson *et al.*, J. Appl. Phys. **99**, 08P703 (2006).
[17] C. B. R. Jesus, M. M. Piva, P. F. S. Rosa, C. Adriano, and P. G. Pagliuso, J. Appl. Phys. **115**, 17E115 (2014).
[18] K. W. H. Stevens, Proc. Phys. Soc. Sec. A **65**, 209 (1952).
[19] S. Süllow, B. Becker, A. de Visser, M. Mihalik, G. J. Nieuwenhuys, A. A. Menovsky, and J. A. Mydosh, J. Phys. Condens. Matter **9**, 913 (1997).
[20] A. Galatanu, Y. Haga, T. D. Matsuda, S. Ikeda, E. Yamamoto, D. Aoki, T. Takeuchi, and Y. Onuki, J. Phys. Soc. Jpn. **74**, 1582 (2005).
[21] K. P. Belov, A. S. Dmitrievskii, A. Zygmunt, R. Z. Levitin, and V. Trzebiatowski, ZhETF **64**, 582 (1973) [JETP **37**, 297 (1973)].
[22] B. Bleaney and R. W. Hill, Proc. Phys. Soc. **78**, 313 (1961).
[23] J. Bieroń and P. Pyykkö, Phys. Rev. Lett. **87**, 133003 (2001).
[24] V. T. Rajan, Phys. Rev. Lett. **51**, 308 (1983).
[25] N. Cao, J. D. Garrett, T. Timusk, H. L. Liu, and D. B. Tanner, Phys. Rev. B **53**, 2601 (1996).
[26] P. Aynajian, E. H. da Silva Neto, C. V. Parker, Y. Huang, A. Pasupathy, J. Mydosh, and A. Yazdani, Proc. Natl. Acad. Sci. U.S.A. **107**, 10383 (2010).
[27] A. D. Christianson, E. D. Bauer, J. M. Lawrence, P. S. Riseborough, N. O. Moreno, P. G. Pagliuso, J. L. Sarrao, J. D. Thompson *et al.*, Phys. Rev. B **70**, 134505 (2004).
[28] D. Kaczorowski and J. Schoenes, Solid State Commun. **74**, 143 (1990).

[29] N. H. Andersen, *Crystalline Field and Structural Effects in f-Electron Systems* (Plenum Press, New York, 1980).

[30] P. F. S. Rosa, C. B. R. Jesus, C. Adriano, Z. Fisk, and P. G. Pagliuso, J. Phys. Conf. Ser. **592**, 012063 (2015).

[31] P. F. S. Rosa, R. J. Bourg, C. B. R. Jesus, P. G. Pagliuso, and Z. Fisk, arXiv:1508.02116.

[32] S. Araki, N. Metoki, A. Galatanu, E. Yamamoto, A. Thamizhavel, and Y. Onuki, Phys. Rev. B **68**, 024408 (2003).